

HIGH-BRIGHTNESS, HIGH-CURRENT-DENSITY CATHODE FOR INDUCTION LINAC FELS*

W. C. Turner, Y.-J. Chen, and W. E. Nexsen
Lawrence Livermore National Laboratory
Livermore, California 94550

M. C. Green, G. Miram, and A. V. Nordquist
Varian Associates
Palo Alto, California 94303

We have recently initiated an investigation to determine the intrinsic operating limits of an osmium coated dispenser cathode for use in free-electron lasers (FELs) driven by an induction linear accelerator. The experimental apparatus consists of a 5.1-cm-diam osmium coated dispenser cathode driven by a 250-kV, 10- Ω , 35-ns Blumlein pulse line. The pepper pot technique is used to measure intrinsic cathode brightness and uniformity. Recent measurements have yielded brightness values exceeding 1×10^{10} A/m²rad² for current densities up to 140 A/cm². We have also obtained quantitative data on cathode poisoning caused by a number of chemical agents of interest in the induction linac environment.

Introduction

High-power, short-wavelength free-electron lasers (FELs) require high brightness, kiloampere electron beams. Consequently, we have initiated an experimental program to characterize the current density, brightness, and voltage gradient limits of an osmium alloy coated dispenser cathode (a derivative of the M cathode). We are also interested in the vacuum conditions required for high current density operation and the cathode lifetime. This type of cathode has been in use for many years in high power microwave tubes. However, their use in the pulsed environment of an induction linac FEL and the emphasis on brightness are relatively new. In this paper we report the extension of our earlier brightness measurements¹ from a current density of 44 A/cm² to 137 A/cm² and also give some initial results of our cathode poisoning tests.

Experimental Setup

A diagram of the experimental setup is shown in Fig. 1. The cathode is a 5.1-cm-diam sintered tungsten disk that has been impregnated with 6BaO-CaO-2Al₂O₃ and coated with approximately 4000 \AA of osmium alloy. The cathode is directly heated with a bifilar spiral-wound filament and is recessed 0.25 cm behind a surrounding water-cooled electrode to suppress edge emission. The anode is a 0.15-cm-thick water-cooled copper plate 2 cm in front of the cathode. The anode has been perforated with a pepper pot pattern of 0.1-mm-diam holes. Beamlets defined by the holes drift 23.5 cm to a 25- μ m aluminum foil that is back coated with ZnO(Ga) phosphor (decay time 0.4 ns). The pepper pot holes lie on 45 $^\circ$ radial lines from the center with the first set spaced 1 cm from the center hole and the rest spaced at 0.5-cm intervals. The phosphor is viewed with a gated-image intensifier CCD camera, and the images are recorded digitally

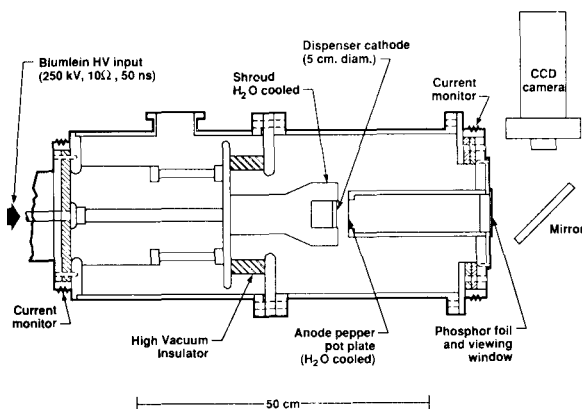


Figure 1. Schematic of the experimental apparatus.

for analysis (0.0174-cm/pixel x direction, 0.0148-cm/pixel y direction). The gate pulse width applied to the microchannel plate is 5 ns. The timing of the gate pulse is adjusted for the peak of the diode voltage and current. An optical pyrometer determines the cathode temperature. Diode voltage and current are measured with a capacitive probe and resistive current monitors, respectively. The diode is driven with a 250-kV, 10- Ω , 35-ns Blumlein pulse line. Vacuum pressure with the cathode hot is 1.0×10^{-7} Torr, and residual gases consist almost entirely of water vapor. For quantitative poisoning experiments we have added a variable leak valve for admitting controlled partial pressures of selected vapors. Partial pressure of a selected vapor is determined by monitoring the current output of a quadrupole residual gas analyzer set on a characteristic mass peak. The absolute sensitivity of the gas analyzer is established by comparison with a capacitance manometer.

Experimental Results

Figure 2 shows a photograph of a recorded pepper pot image redisplayed on a video monitor. The diode voltage for these data was 106 kV and the space charge limited current 436 A. The images of the individual holes are well separated, and there is no apparent elongation in the radial direction from energy variations since the camera gate pulse is short (5 ns) and timed to occur at peak voltage, where variation in beam energy is small. The regular pattern is also characteristic of space-charge-limited current. For currents below the space-charge limit the image pattern of the anode holes becomes quite distorted. Because the anode plate shorts out the radial space charge electric field at the anode, the beam magnetic field causes the beam to pinch inward. This is evident in Fig. 3, where we have plotted beamlet direction (mean x') versus x at $y = 0$ projected back to the anode. The S shape of this curve also indicates some nonlinearity in the focusing force. Because of this inward pinching the hole images get too close together for their radii to be measured easily at beam energies much above 106 keV. For this reason brightness data above 106 keV are taken with a single central hole in the anode. In the future we may move the phosphor closer to the anode to obtain multi-hole images for energies greater than 106 keV.

A profile of image intensity versus radial position of pepper pot holes in the anode is shown in Fig. 4(a) for a beam voltage $V = 106$ kV. Both the raw data and the data corrected for beam scrape off due to noncollinearity of the hole axis and beamlet direction are shown in Fig. 4(a). Similarly a profile of beamlet intensity versus azimuth at 1-cm radius is shown in Fig. 4(b). Azimuthally the beamlet intensity appears uniform to $\pm 15\%$. The edge of the beam is not particularly well resolved since the spacing between holes is 0.5 cm and the measurements at $r = 2.5$ cm are sensitive to small misalignments. Since we have not independently verified the uniformity of the phosphor and cathode we can only say that the cathode current density is at least as uniform as the intensity plotted in Fig. 4.

For each beamlet image on the phosphor we define an image radius a equal to the radius of a circle that encloses 90% of the electrons. Beamlet divergence angle is then calculated as $\theta = a/l$, where $l = 23.5$ cm, the distance between the anode and phosphor. The procedure is indicated in Fig. 5, where we give intensity scans through a single spot in two orthogonal directions. A background intensity I_{bkg} is subtracted from the data and the full width of the curves read off at an intensity $I = 0.135(I_{\text{max}} - I_{\text{bkg}})$ and set equal to $2a$. This corresponds to the 2σ level of a Gaussian, which fits the data quite well and which encloses 90% of the electrons.

Figure 6 shows beamlet divergence angle versus anode radius for the data used for Fig. 4. Within $\pm 10\%$, the divergence angle is constant and independent of radius. We have also verified that the

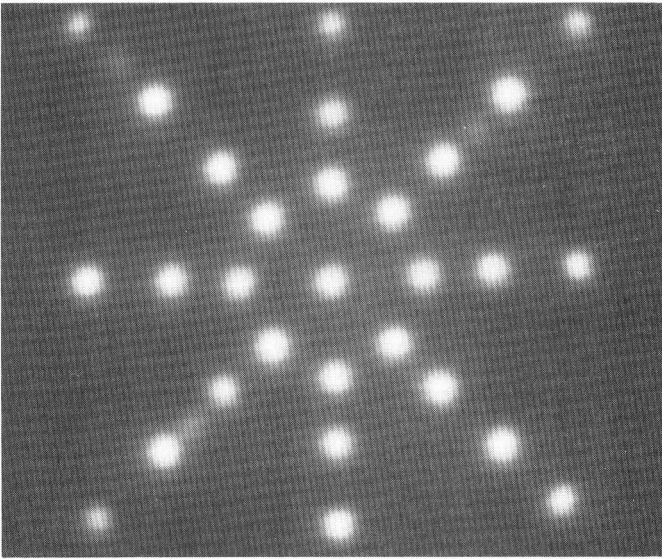


Figure 2. Photograph of digitally recorded pepper pot image.

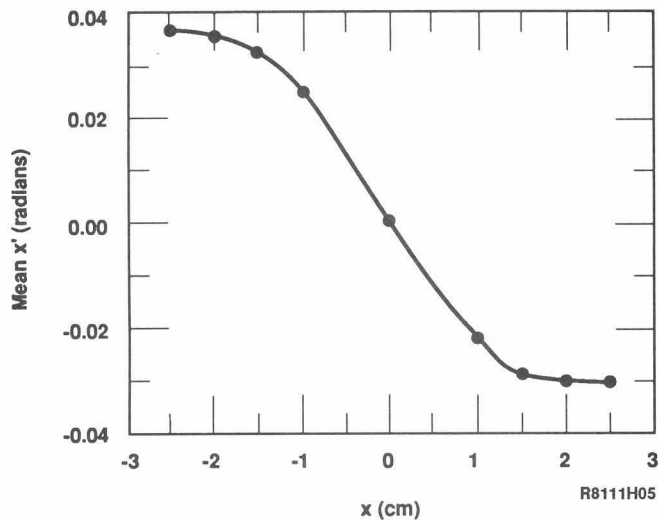


Figure 3. Mean x' versus x at $y = 0$.

beamlet images are circular by comparing radial widths of intensity profiles in orthogonal directions.

In addition to the divergence caused by random perpendicular velocity spread, which is the object of our measurement, a number of other effects contribute to the divergence angles measured in Fig. 6. These include camera resolution (θ_{cam}), defocusing by field penetration into the anode holes defining the beamlets (θ_{hole}), and space charge (θ_{sc}). Estimates of each effect are given in Table 1 together with the raw data (θ_{meas}) and the corrected divergence angle (θ_b) we used to estimate brightness. Additional contributions from finite source size and change of mean beamlet steering angle across the anode holes are negligible. We measured the angular spread arising from finite camera spatial resolution (θ_{cam}) by fitting a Gaussian function to the intensity distribution at the edge of a uniformly illuminated white spot. The divergence angle from hole defocusing (a_0) is calculated from the hole size and anode cathode separation (d) for the space-charge-limited case: $\theta_{\text{hole}} = 2/3[\gamma/(\gamma + 1)]a_0/d$. Using a method similar to that of Oettinger et al.,² we determine the space charge contribution from the first integral of a beam envelope equation for a beamlet passing from the anode to the phosphor. The final result for the corrected beam divergence angle is then obtained

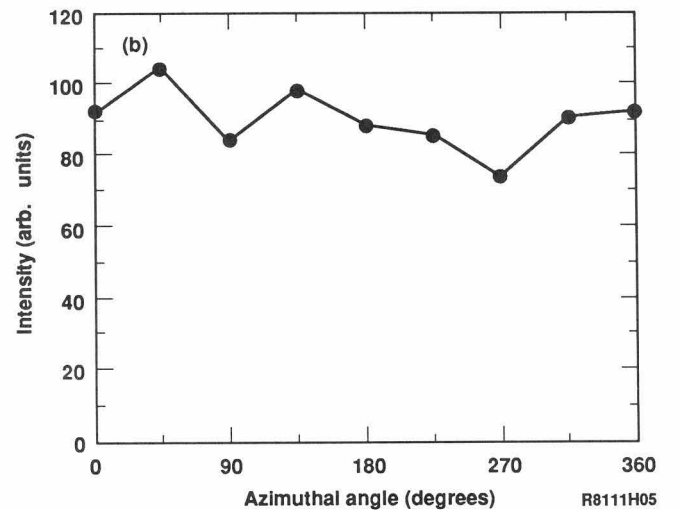
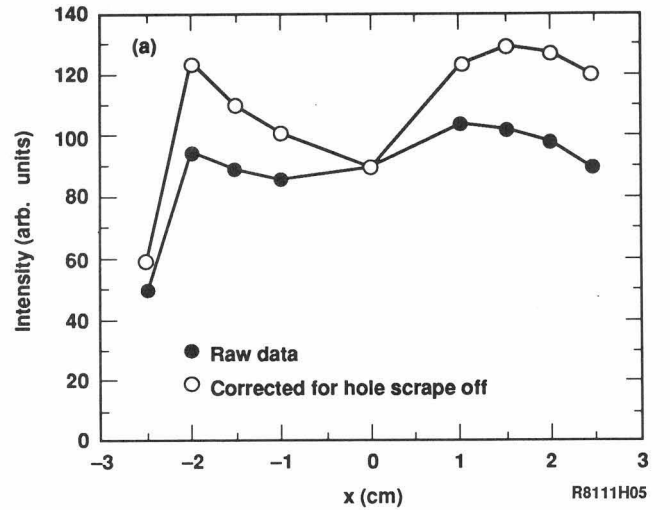


Figure 4. (a) Beamlet image intensity versus x . (b) Beamlet image intensity versus azimuthal angle at $R = 1$ cm.

from $\theta_b = (\theta_{\text{meas}}^2 - \theta_{\text{cam}}^2 - \theta_{\text{hole}}^2 - \theta_{\text{sc}}^2)^{1/2}$. As seen from Table 1 the corrected divergence is about 25% less than the measured value.

To estimate cathode brightness from our data we use the definition³

$$J = I/(\beta\gamma)^2 V_4$$

where V_4 is the four-dimensional phase space volume occupied by the electrons. Since the beam divergence angle is independent of radius, as shown in Fig. 6, to good approximation $V_4 = \pi R_c^2 \times \pi \theta_b^2$ and

$$J = I/\pi^2(R_c\beta\gamma\theta_b)^2$$

where $R_c = 2.54$ cm is the cathode radius.

Estimates of brightness are summarized in Table 2 for five sets of data obtained from a diode voltage of 106 kV to 407 kV and corresponding current densities varying from 21.5 A/cm² to 137 A/cm². When gathering these data we took care to assure operation above the knee of the transition from temperature to space-charge-limited flow. The perveance (12.6×10^{-6} A/V^{3/2}) is within 5% of the Child-Langmuir equation. The cathode temperature was 1100°C_B for the 106-kV data and 1300°C_B for 407 kV. Although the current density varies by a factor of 6.4 in Tables 1 and 2 the brightness lies in a relatively narrow range $1.14\text{--}1.6 \times 10^{10}$ A/m²rad². This result is a consequence of the weak variation of θ_b with diode voltage. If there were a single transverse thermal energy characteristic

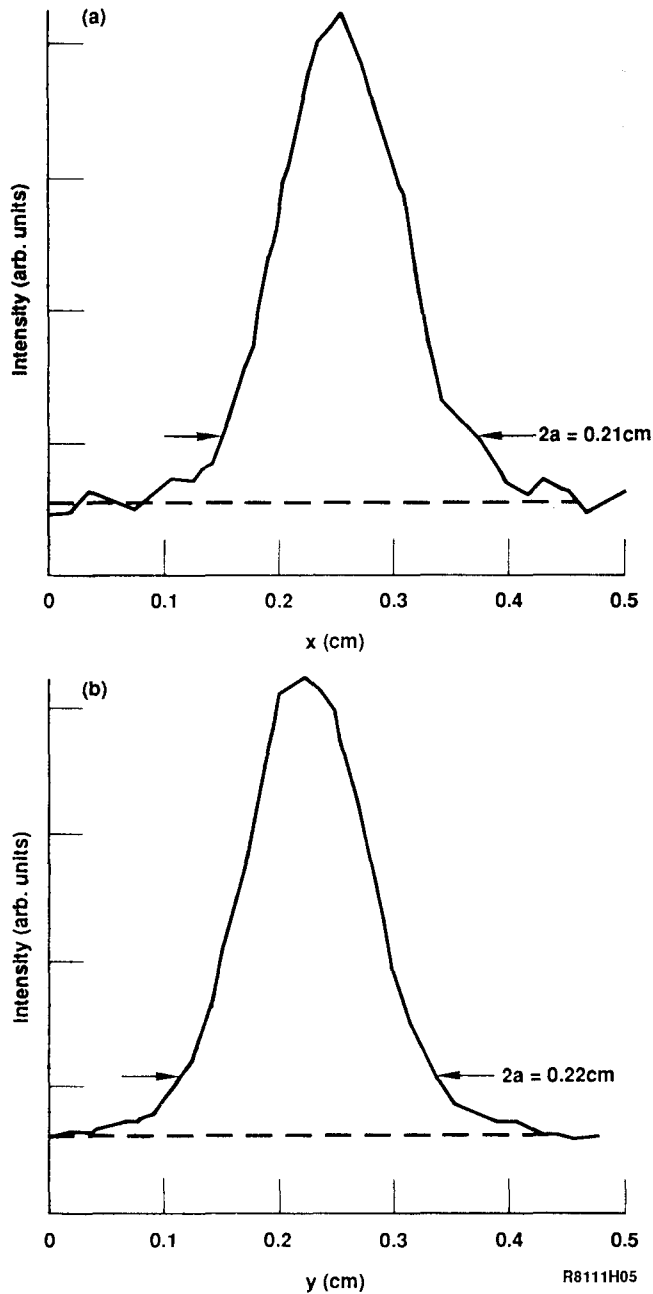


Figure 5. Intensity profiles of a single beamlet image (a) versus x at $y = 0$ and (b) versus y at $x = 0$.

of the cathode, then one would expect $\beta\gamma\theta_b$ to be a constant that is independent of diode voltage. However it is apparent from the third column of Table 2 that this is not what is observed. The transverse thermal energy of the beam, defined to be $E_{\perp} = 1/2mc^2(\beta\gamma\theta_b)^2$, is 1.5 eV for $V = 106$ kV and increases to 9.2 eV for $V = 407$ kV. For this initial set of data we have not yet identified the origin of this transverse energy nor have we established the upper bound of practically attainable high-brightness, high-current-density operation.

We have begun to look at the sensitivity of the cathode to poisoning by various chemical compounds. In this paper we report results obtained on poisoning by the dominant constituents of a leak-tight, unbaked vacuum system—water vapor, carbon monoxide, and methane. Typically the background partial pressure for water vapor is 1×10^{-7} Torr and considerably less for carbon monoxide and methane. What we found was that the cathode emission current begins to decrease with only a slight increase in the partial pressure of water vapor, whereas such a decrease is not observed until a

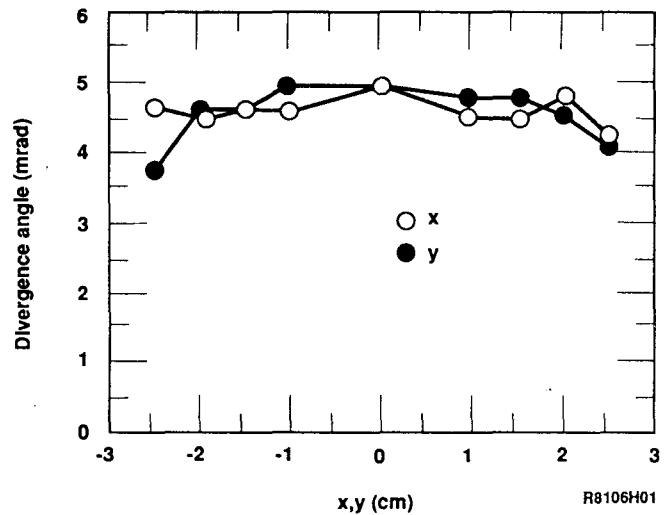


Figure 6. Beamlet divergence angle versus x, y .

Table 1. Summary of beamlet divergence angles.

W (keV)	$\gamma\beta$	θ_{meas} (mrad)	θ_{cam} (mrad)	θ_{hole} (mrad)	θ_{sc} (mrad)	θ_b (mrad)
106	0.676	4.68	2.38	0.92	1.51	3.62
172	0.888	4.47	2.38	0.95	1.60	3.29
269	1.15	4.94	2.38	1.00	1.69	3.86
384	1.44	5.11	2.38	1.07	1.75	4.03
407	1.49	5.11	2.38	1.07	1.75	4.03

Table 2. Summary of brightness results.

W (keV)	I (A)	$\gamma\beta\theta_b$ (rad)	$R_c\gamma\beta\theta_b$ (m-rad)	J ($\text{A}/\text{m}^2\text{rad}^2$)
106	436	2.45 E-3	6.22 E-5	1.14 E10
172	889	2.92 E-3	7.42 E-5	1.64 E10
269	1564	4.44 E-3	1.13 E-4	1.24 E10
384	2594	5.80 E-3	1.47 E-4	1.22 E10
407	2780	6.00 E-3	1.52 E-4	1.22 E10

partial pressure of 1×10^{-5} Torr is reached for carbon monoxide, and no decrease was observed for methane up to 1×10^{-4} Torr. The poisoning curve for water vapor is shown in Fig. 7. The cathode emission current recovers when water vapor pressure is reduced to its background level. If we increase the cathode temperature, then the partial pressure at which the emission current decreases is observed to increase. What this implies is that the background water vapor pressure in our system is causing an effective increase of work function, and therefore we need to operate the cathode somewhat hotter (approximately 40°C) than if the water vapor pressure were reduced by about an order of magnitude. We note, however, from the data of Table 2 that quite good emission current densities and brightnesses are obtainable with this type of cathode in an unbaked vacuum system.

Discussion

In Fig. 8 we plot cathode brightness versus current for the data obtained in this paper and for several other cathodes recently examined in the FEL context—graphite and velvet field emission cathodes,^{4,5} a Cs_3Sb photocathode,^{2,6} and a LaB_6 thermionic cathode.⁷

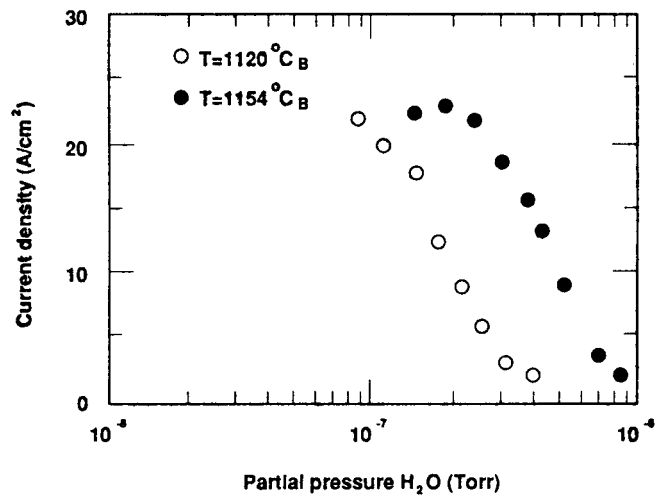


Figure 7. Cathode current density versus partial pressure of water vapor.

Of course, many other factors enter into the choice of cathode for a particular application. For instance, graphite and velvet field emission cathodes cannot be operated at high repetition frequencies, whereas the others can. Only the Cs₃Sb cathode is easily gated after application of a high voltage pulse to the diode. Graphite and velvet can operate in poor vacuum conditions, Cs₃Sb requires the best vacuum conditions (10⁻¹⁰ Torr), LaB₆ is relatively insensitive to poisoning and can operate at 10⁻⁶ Torr, and the osmium coated dispenser cathode can operate at 10⁻⁷ Torr.

So far we have not identified the practical upper limit on current density for the osmium-coated dispenser cathode in the induction linac environment. Ultimately, high current density operation will be limited by too short cathode lifetime at high temperature or by undesirable field emission from the cold electrode that surrounds the cathode. For data in this paper the maximum field stress on the cold electrode was 200 kV/cm, and field emission was not evident in surface damage or pulses with a cold cathode. The data in this paper were limited by the maximum operating voltage of the Blumlein pulse line. In the future we will increase the voltage stress by decreasing the diode gap from 2 cm to 1.0 cm.

To use the cathode studied here in an injector we will need to modify the electrode structure to permit the beam to be extracted through a hollow anode. This will necessitate decreasing the perveance from approximately 11 to 1.5 μ pervs. Since for constant cathode current and radius the electric field stress is proportional to the inverse one-sixth power of perveance this will result in a 37% increase in field stress on the cold electrode surrounding the cathode. A second crucial issue is how much the beam brightness will be degraded by extraction through the hollow anode.

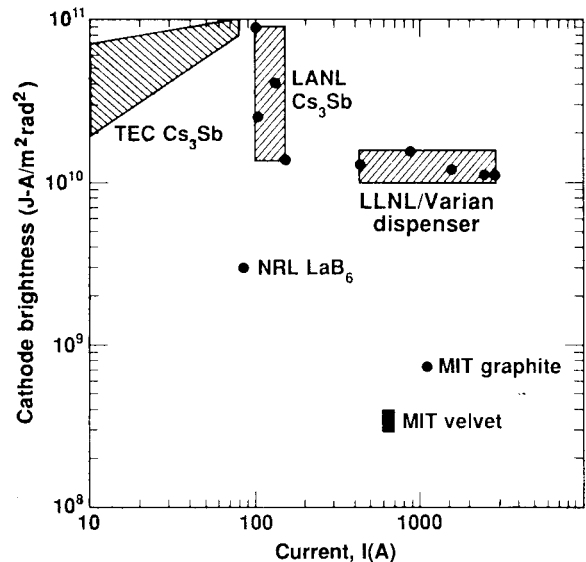


Figure 8. Cathode brightness versus current for various cathodes.

References

1. W. C. Turner, Y.-J. Chen, M. C. Green, G. V. Miram, and A. L. Nordquist, *Proc. Beams '88 Seventh Intl Conf High Power Particle Beams*, Karlsruhe, Federal Republic of Germany, July 4-8, 1988 (in press).
2. P. E. Oettinger, I. Bursac, R. E. Sheffer, and E. Pugh, *Proc. 1987 IEEE Particle Accelerator Conf.*, Washington, DC., 286-288.
3. C. Lejeune and J. Aubert, in *Applied Charged Particle Optics*, A. Septier, Ed. (Academic Press, New York, 1980), Part A, 159-259.
4. D. A. Kirkpatrick, R. E. Shefer, and G. Bekefi, *J. Appl. Phys.* **57**(11), 5011 (1985).
5. F. Hartmann, G. Bekefi, D. A. Kirkpatrick, R. E. Klinkowstein, and R. E. Shefer, *Proc. 1987 IEEE Particle Accelerator Conf.*, Washington, D.C., pp. 385-387.
6. J. S. Fraser, R. L. Sheffield, E. R. Gray, P. M. Giles, R. W. Springer, and V. A. Loeb, *ibid.*, pp. 1705-1709.
7. P. Loschialpo and C. A. Kapetanakis, *High-Current Density, High Brightness Electron Beams from Large-Area Lanthanum Hexaboride Cathodes*, NRL Memorandum 6119, Naval Research Laboratory, December 13, 1987.

*Performed jointly under the auspices of the US DOE by LLNL under W-7405-ENG-48 and for the DOD under SDIO/SDC-ATC MIPR No. W31RPD-8-D5005.